International Journal on Advanced Science Engineering Information Technology

Vol.11 (2021) No. 5
ISSN: 2088-5334

Utilization of Band Combination for Feature Selection in Machine Learning-Based Roof Material Types Identification

Ayom Widipaminto [a,b,*], Yohanes Fridolin Hestrio [a], Donna Monica [a], Yuvita Dian Safitri [a], Dedi Irawadi [a], Rokhmatuloh [b], Djoko Triyono [b], Erna Sri Adiningsih [a]

[a] *Remote Sensing Technology and Data Center, National Institute of Aeronautics and Space, Jakarta Timur, 13710, Indonesia*
[b] *Physics Department, Faculty of Mathematics and Sciences, University of Indonesia, Depok, 16424, Indonesia*
Corresponding author: [*]ayom.widipaminto@lapan.go.id

***Abstract*— Land monitoring requires remote sensing data, which varies in its spectral and spatial resolution. Remote sensing data with the high spatial resolution is especially needed for urban monitoring. However, high spatial resolution data is usually expensive with limited coverage and complex analysis. This paper aims to find the most efficient way to do urban monitoring, specifically surface material identification. In material identification, the distinctive feature that can be used to differentiate one material surface from one another is its reflectance responses. This leads to a question of which absorption features are significant to different surface materials, especially roofing materials, and which absorption features are not discriminant enough to be used at classification. This paper proposed a machine learning-based identification of roof material types using band combinations as classification features. The experiment was done on Pleiades data, multispectral satellite imagery with very high spatial resolution. We first calculated the image's reflectance values for each band and then grouped them based on their spectral range, yielding 11 possible combinations as the classification features. The experiment found that reflectance responses for band Red and NIR are the most distinctive trait of a material type and thus sufficient for material identification. We minimized the number of spectral responses used in material identification down to two bands, which can help the data collection and processing of material identification easier, cheaper, and less time-cost. Our experiment yields overall accuracy of 0.9959, with a computational time of 19.72 seconds.**

***Keywords*—Material identification; band combination; reflectance responses.**

Manuscript received 2 Sep. 2020; revised 27 Feb. 2021; accepted 29 Apr. 2021. Date of publication 31 Oct. 2021.

I. INTRODUCTION

Land monitoring is greatly supported by remote sensing and GIS technology. Both remote sensing and GIS have given us a better perspective about earth's history [1], [2], land changes [3], and urban conditions [4], [5], which are necessary for decision making [6]–[8]. Remote sensing data that can be used for land monitoring varies in its spectral and spatial resolution. Urban monitoring, however, requires high spatial resolution, and therefore, airborne data is commonly used as the standard data for urban monitoring. Airborne data is usually expensive with limited coverage and complex analysis [9] and still needs to be backed up by satellite data which availability has been increasingly growing and can cover both local [10] and global monitoring [11].

In urban monitoring, one of the important information that can be obtained is the type of material used in urban objects. They can give great insights into urban conditions such as urban building's vulnerability toward disaster [12], potential green space [13], regional sustainability [14], and urban climate [15]. Many types of research related to urban materials have been done before and continue. Building surface materials have been identified using hyperspectral imagery and many methods, such as normalized difference plastic index to identify plastic material in a natural and urban environment [16], Build-up Surface Index and Build-up Area Extraction Index to detect road surfaces [17], and dual-stage convolutional networks to identify road materials [18]. Another research has differentiated rooftops from non-rooftops based on the image's grey level using segmentation, SVM classification, and histogram [19]. City mapping has also been done using spectroscopy data from EnMAP hyperspectral spaceborne imaging [20].

Meanwhile, methods commonly used for identification or classification are Support Vector Machine (SVM) and Random Forest (RF). SVM [21] has been widely used for text classification [22], object identification [23], and handwriting

recognition [24], as it has an excellent theoretical foundation and empirical success. While RF is an ensemble classifier based on randomization, it makes predictions by averaging over several independent base models [25], [26]. Wainberg found no significant difference between the Random forest and the SVM method [27]. This shows that there is no absolute best machine learning method because it depends on each study case. Both SVM and RF can yield high accuracy of classification [28], and it comes down to finding the right feature to be used in the method to optimize the classification process and result.

In material identification, the distinctive feature that can be used to differentiate a material surface from one another is its absorption features and reflectance [29]. Each material produces particular reflectance patterns that play a role as the material's signature [30]. These reflectance characteristics of material surfaces can be analyzed using remote sensing imagery's spectral bands. A single remote sensing image can have many spectral bands taken by many sensors, which is redundant computational-wise and expensive in obtaining it [31]. This leads to a question of which absorption features are significant to different surface materials, especially roofing materials, and which absorption features are not discriminant enough to be used at classification.

The imagery in previous studies was used as the dataset is commonly hyperspectral images [16]–[20]. The usage of those hyperspectral images is expensive and brings much complexity to the computation and is redundant as the hyperspectral images have hundreds of bands, and not all of them are significant for the computation. This paper aims to find the most efficient spectral bands that can be used to classify materials. We want to find the least number of bands sufficient to classify the material, simplify the computation, and make obtaining data more efficient while still maintaining the accuracy of the classification. This paper proposed a machine learning-based identification of roof material types by selecting the most optimized features [31] in such a way that results in the most accurate roof classification. The identification will be made on Pleiades data, multispectral satellite imagery with very high spatial resolution. Many urban objects that are characteristic of urban structures can be recognized in the identified surface material map. To avoid the common problem of small buildings and streets being overshadowed by trees and other vegetation, we will first apply vegetation masking before the classification. Using masking is an advantage for reducing the confusion between roof and ground materials [32]. The rest of the paper is organized as follows. Section 2 describes the materials and methods we proposed. Section 3 explains the experiment results and discussion. Section 4 concludes the finding of this research and future works.

II. Material and Method

A. Material

The study area is located on the office building of Remote Sensing Technology and Data Center, LAPAN, and its surrounding area in Pekayon, East Jakarta. The office building has various material types forming its rooftops, such as aluminum, asbestos, ceramic tiles, concrete, and sand metal tiles. This research uses 4-band orthorectified Pleiades 1A data, which captured the study area in May 2018. Pleiades image that we use in this research has a multispectral product that includes four multispectral bands: Blue, Red, Green, and Near-Infrared. The product pixel size is 2 m [33]. We chose a scene with a requirement of 0% for cloud cover and less than 20% for viewing angle. A quick look at the data is shown in Figure 1.

B. Method

Our proposed method consists of three stages: the initial, implementation, and final stages. The initial stage is where the data is prepared. The preparation is done by applying the pan-sharpening method to the Pleiades imagery data. Pan sharpening [34] is a method to increase an image's spatial resolution employing resampling. We use Ehlers's method [35] to increase the data's spatial resolution from 2m to 50cm.

The implementation step is where we process the data for classification, which consists of five steps. The first step is applying vegetation masking to remove vegetation such as trees and shrubs from the data. This step is necessary to prevent the vegetation's spectral responses from influencing the classification of buildings and other urban objects. The masking method used in this research is a threshold method based on the normalized difference vegetation index (NDVI). We calculate the NDVI value of each data pixel to separate the vegetation from the urban objects. The higher an NDVI value of a pixel, the higher probability of said pixel is representing vegetation. We use trial and error to determine the threshold value for NDVI that separates the vegetation and non-vegetation.

Fig. 1 Multispectral data from Pleiades satellite for the Remote Sensing Technology and Data Center Office and the roof material in the existing housing in the Pekayon district around the office

The second step is obtaining the training data used in classification using the cluster sampling method [36]. We randomly choose five clusters from the dataset based on their materials and do a systematic sampling for each cluster to obtain the pixels used as the training data. We select five clusters of pixels representing aluminum, asbestos, ceramic tiles, concrete, and sand metal tiles.

The third step is extracting features from the training data by converting the digital values of pixels in each band into reflectance values. The reflectance value of each pixel of the data can be calculated by considering the digital number of each pixel, the radiometric gain value of the image, and the

sun elevation angle. Those values are retrieved from the image and the image's metadata. The equation we used to obtain the reflectance values is referred to Astrium [37]. Since Pleiades imagery is multispectral with red, green, blue, and NIR bands, we will have four spectral responses for every material we classify.

The fourth step is grouping the four bands of the Pleiades dataset, based on Li [31], which has made the feature selection by grouping all the bands based on their spectral range. We combined every pair, yielding in 11 combinations, which are Blue-NIR, Blue-Red, Blue-Green, Red-NIR, Red-Green, Green-NIR, Red-Green-Blue, Red-Green-NIR, Red-Blue-NIR, Green-Blue-NIR, and Red-Green-Blue-NIR.

After obtaining the features, the fifth step is developing the classification model using Random Forest (RF) method. We choose RF as the classification method as pointed out by [38] that RF is more fitted and reliable for practical and complicated applications. The process is run on R, where we set the number of trees n = 14, and training data 70% of total data. First, we will conduct training to find the classification model and then use the classification model to classify the rest of the data, producing five classes of materials, namely aluminum, asbestos, ceramic tiles, concrete, and sand metal tiles.

Finally, the last stage is evaluation, in which we compare and evaluate the classification results to find the most efficient feature. The parameters used for evaluations are classification accuracy and computational time. The flowchart of the proposed method can be seen in Figure 2.

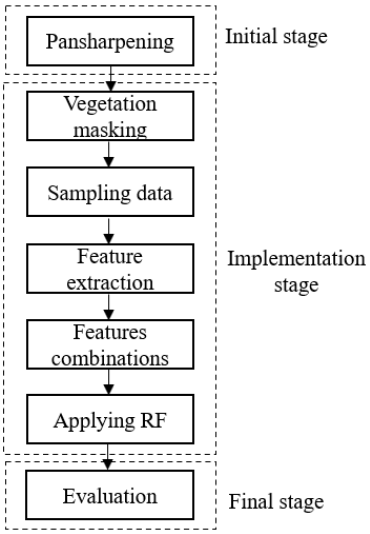

Fig. 2 Flowchart of the proposed method

III. Results and Discussion

For the initial stage, we did a pan sharpening using Ehlers method and Ermapper software. This process increased the data's spatial resolution from 2m to 50cm. We used the NDVI threshold through several trials for the masking before obtaining a fixed value of 0.3 as the threshold. It means that pixels with NDVI value 0.3 and above are considered vegetations and therefore removed from the data, leaving only the urban objects that will be classified. The urban-only, pan-sharpened data can be seen in Figure 3 and Figure 4.

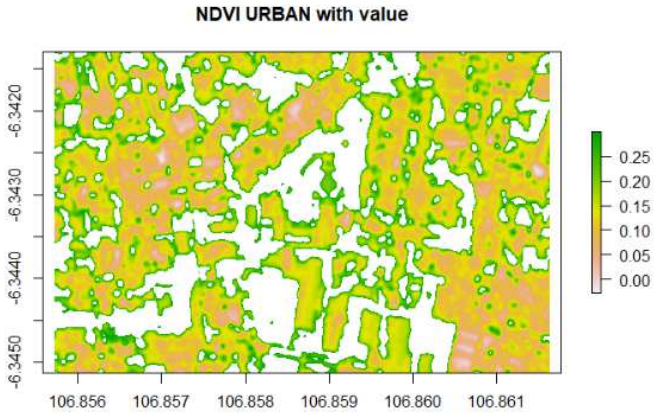

Fig. 3 NDVI value of each pixel in which value more than 0.3 considered vegetation

Fig. 4 Vegetation masking result

We then selected the training data from the masked image. We randomly chose five clusters and systematically selected pixels of the same distances from each cluster. The five clusters represent ceramic tile, concrete, asbestos, sand metal tile, and aluminum. We gained 734 data points for each type of aluminum, asbestos, ceramic tiles, concrete, and metal sand tiles. The data points consist of 114 data points for aluminum, 119 data points for asbestos, 143 data points for ceramic tile, 42 data points for concrete, and 316 data points for sand metal tile.

After collecting the training data, we converted the pixels' value of all the data points from those training data into the reflectance value. From this step, we obtained the average value of each material's spectral responses toward every band in our dataset, namely the Blue, Green, Red, and NIR band. Then, we implemented the classification. We used a machine learning approach with the Random Forest method. From our previous 734 data sampling, we use 70% of them as the training data and the rest as the test data. The classification process was conducted eleven times with different feature selection in each process.

TABLE I
Spectral Responses for Each Material

Material Types	Blue	Green	Red	NIR
Aluminum roof	0.3223559	0.2991867	0.2764054	0.3340441
Asbestos	0.2340635	0.2042975	0.1835748	0.2377383
Ceramic tile	0.2154938	0.1842477	0.1927679	0.2600768
Concrete	0.3174365	0.2753749	0.2531401	0.3905671
Sand metal tile	0.2204477	0.1872178	0.1677609	0.2228527

First, we used all the Pleiades bands as features for the RF method. We obtained model accuracy 0.9746468, overall accuracy 1, Kappa value 0.9648743, and computational time 35.63 seconds for one data. In the second experiment, we lessened the number of bands into three. There are four combinations of bands which are Red-Green-Blue, Red-Green-NIR, Red-Blue-NIR, and Green-Blue-NIR. Each combination is used as a feature in the classification. The accuracy, Kappa value, and time consumption for each model are shown in Table 2.

TABLE II
ACCURACY COMPARISON OF 3-BAND COMBINATIONS

Band Grouping	Accuracy		Kappa		Time (s)
	Model	Overall	Model	Overall	
Red-Green-Blue	0.962423	1	0.948125	1	26.23
Red-Green-NIR	0.971148	1	0.959979	1	25.89
Red-Blue-NIR	0.949229	1	0.930321	1	26.9
Green-Blue-NIR	0.958583	1	0.934609	1	26.42

From Table 2 we can conclude that the best feature among the 3-band combinations is the Red-Green-NIR combination with model accuracy 0.971148, overall accuracy 1, and computational time 25.89 seconds. The accuracy of the model is only 0.36% lower than the all-band feature model, and the overall accuracy does not decrease. Meanwhile, the computational time is shorter by 27.37%. Finally, the third experiment, we again lessened the band number into two and implemented the classification six times for every 2-band combination, namely Blue-NIR, Blue-Red, Blue-Green, Red-NIR, Red-Green, and Green-NIR. The result is shown in Table 3. The best accuracy is obtained by the classifier with the Red-NIR feature, which is 0.9361645 for the model accuracy and 0.9959 for the overall accuracy, with computational time 19.72 seconds.

TABLE III
ACCURACY COMPARISON OF 2-BAND COMBINATIONS

Band Grouping	Accuracy		Kappa		Time (s)
	Model	Overall	Model	Overall	
Blue-NIR	0.895232	0.9932	0.8543965	0.9906	20.83
Blue-Green	0.7915978	0.9537	0.7102323	0.9358	22.7
Blue-Red	0.8932299	0.9959	0.8521683	0.9943	20.39
Green-NIR	0.9165679	0.9959	0.8842042	0.9943	19.98
Green-Red	0.8724109	0.9946	0.8225482	0.9925	20.2
Red-NIR	0.9361645	0.9959	0.9118185	0.9943	19.72

The computational time for this model is significantly shorter than the best 3-band featured model by 23.83% and the all-band featured model by 44.65%. Accuracy-wise, the model accuracy for this classifier with the Red-NIR feature is lower than the one with the Red-Green-NIR feature by 3.60% and the one with the all-band feature by 3.95%. As for the overall accuracy, it decreases slightly by 0.41%. The classified image resulted from the Red-NIR featured model is shown in Figure 5.

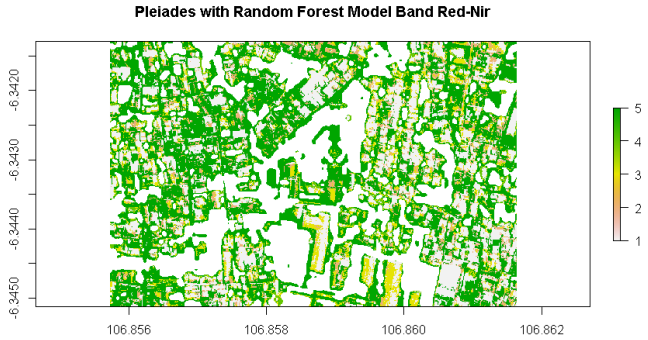

Fig. 5 Classification result for Red-NIR band featured model

The experiment results show that the classifier with the Red-NIR band combination as its feature gives the best efficiency. The computational time is the shortest among other features, and the number of bands can be minimized into two bands only, which makes it easier and cheaper to collect spectral responses data. Moreover, although the accuracy is decreasing, the difference between the Red-NIR's model accuracy and the highest model accuracy is under 4% while the difference in overall accuracy is under 1%, which is still acceptable. It can also be seen from Table 2 that the Blue-Green combination yields the lowest accuracy, which further supports the finding that the Red and NIR spectral responses are the most distinguishable trait of material types and those two only suffice to differentiate material types from one another.

IV. CONCLUSIONS

This research found that spectral responses for band Red and NIR are the most distinguishable trait of a material type and thus sufficient for material identification. We minimized the number of spectral responses used in material identification down to two bands, which can help data collection in future material identification easier and cheaper. We applied our model to classify the roof material of the Remote Sensing Technology and Data Center Office and the roof material in the existing housing in the Pekayon district around the office. Using the Random Forest method feature selection from the Red-NIR band, we obtained model accuracy 0.9361645 and overall accuracy 0.9959 with a computational time 19.72 seconds. This computational time is significantly shorter than the best 3-band featured model by 23.83% and the all-band featured model by 44.65%. Although the accuracy also decreases, the difference between the Red-NIR's model accuracy and the highest model accuracy is under 4%, while the difference in overall accuracy is under 1%, which is still acceptable.

For future work, we plan to add a specular correction to the data before the processing and identification to increase the identification accuracy. We also plan to fuse high-resolution data with medium resolution data to investigate the effect of higher infrared wavelengths on the identification within the same resolution.

ACKNOWLEDGMENT

This research was supported by PRN Research Grant 256/E1/PRN/2020 from the Ministry of Research and Technology - National Research and Innovation Agency, and

PUTI NKB-1633/UN2.RST/HKP.05.00/2020 from Universitas Indonesia.

AUTHOR CONTRIBUTIONS

AW conceived, planned the experiments, and took the lead in writing the manuscript. YFH carried out the experiments and the simulations. DM and YDS contributed to sample preparation, interpretation of the results, and writing the manuscript with all authors' input. DI contributed to the recommendations for the use of data. R, DT, and ESA helped to review the paper and methodology. DI, R, DT, and ESA also helped supervise the project and encourage AW, YFH, DM, YDS to investigate and supervise this work's findings. All authors provided critical feedback and helped shape the research, analysis, and manuscript.

REFERENCES

[1] Y. Jamei, P. Rajagopalan, and Q. C. Sun, "Time-series dataset on land surface temperature, vegetation, built up areas and other climatic factors in top 20 global cities (2000–2018)," *Data Br.*, vol. 23, p. 103803, 2019, doi: https://doi.org/10.1016/j.dib.2019.103803.

[2] X. Zhang, J. Yao, J. Wang, and K. Sila-Nowicka, "Changes of forestland in China's coastal areas (1996-2015): Regional variations and driving forces," *Land use policy*, vol. 99, p. 105018, 2020, doi: https://doi.org/10.1016/j.landusepol.2020.105018.

[3] M. Matsa, O. Mupepi, T. Musasa, and R. Defe, "A GIS and remote sensing aided assessment of land use/cover changes in resettlement areas; a case of ward 32 of Mazowe district, Zimbabwe," *J. Environ. Manage.*, vol. 276, p. 111312, 2020, doi: https://doi.org/10.1016/j.jenvman.2020.111312.

[4] J. Yan, W. Zhou, L. Han, and Y. Qian, "Mapping vegetation functional types in urban areas with WorldView-2 imagery: Integrating object-based classification with phenology," *Urban For. Urban Green.*, vol. 31, pp. 230–240, 2018, doi: https://doi.org/10.1016/j.ufug.2018.01.021.

[5] S. Ahmed, "Assessment of urban heat islands and impact of climate change on socioeconomic over Suez Governorate using remote sensing and GIS techniques," *Egypt. J. Remote Sens. Sp. Sci.*, vol. 21, no. 1, pp. 15–25, 2018, doi: https://doi.org/10.1016/j.ejrs.2017.08.001.

[6] J. Magidi and F. Ahmed, "Assessing urban sprawl using remote sensing and landscape metrics: A case study of City of Tshwane, South Africa (1984–2015)," *Egypt. J. Remote Sens. Sp. Sci.*, vol. 22, no. 3, pp. 335–346, 2019, doi: 10.1016/j.ejrs.2018.07.003.

[7] M. Eghtesadifard, P. Afkhami, and A. Bazyar, "An integrated approach to the selection of municipal solid waste landfills through GIS, K-Means and multi-criteria decision analysis," *Environ. Res.*, vol. 185, p. 109348, 2020, doi: https://doi.org/10.1016/j.envres.2020.109348.

[8] S. N. Shorabeh, A. Varnaseri, M. K. Firozjaei, F. Nickravesh, and N. N. Samany, "Spatial modeling of areas suitable for public libraries construction by integration of GIS and multi-attribute decision making: Case study Tehran, Iran," *Libr. Inf. Sci. Res.*, vol. 42, no. 2, p. 101017, 2020, doi: https://doi.org/10.1016/j.lisr.2020.101017.

[9] E. Taherzadeh and H. Z. M. Shafri, "Development of a Generic Model for the Detection of Roof Materials Based on an Object-Based Approach Using WorldView-2 Satellite Imagery," *Adv. Remote Sens.*, vol. 2, pp. 312–321, 2013, doi: 10.4236/ars.2013.24034.

[10] A. G. Copado-Rivera, J. Bello-Pineda, J. A. Aké-Castillo, and P. Arceo, "Spatial modeling to detect potential incidence zones of harmful algae blooms in Veracruz, Mexico," *Estuar. Coast. Shelf Sci.*, vol. 243, p. 106908, 2020, doi: https://doi.org/10.1016/j.ecss.2020.106908.

[11] H. MacDonald and D. McKenney, "Envisioning a global forest transition: Status, role, and implications," *Land use policy*, vol. 99, p. 104808, 2020, doi: https://doi.org/10.1016/j.landusepol.2020.104808.

[12] D. H. Lang, A. Kumar, S. Sulaymanov, and A. Meslem, "Building typology classification and earthquake vulnerability scale of Central and South Asian building stock," *J. Build. Eng.*, vol. 15, pp. 261–277, 2018, doi: https://doi.org/10.1016/j.jobe.2017.11.022.

[13] C. Arunplod, "Detecting the potential roof for green rooftop development using geospatial techniques: A case study in North of Bangkok," *Springer Geogr.*, pp. 12–20, 2020, doi: 10.1007/978-3-030-33900-5_2.

[14] Y. Liu, J. Li, L. Duan, M. Dai, and W. Chen, "Material dependence of cities and implications for regional sustainability," *Reg. Sustain.*, vol. 1, no. 1, pp. 31–36, 2020, doi: https://doi.org/10.1016/j.regsus.2020.07.001.

[15] M. Hendel, S. Parison, A. Grados, and L. Royon, "Which pavement structures are best suited to limiting the UHI effect? A laboratory-scale study of Parisian pavement structures," *Build. Environ.*, vol. 144, pp. 216–229, 2018, doi: https://doi.org/10.1016/j.buildenv.2018.08.027.

[16] X. Guo and P. Li, "Mapping plastic materials in an urban area: Development of the normalized difference plastic index using WorldView-3 superspectral data," *ISPRS J. Photogramm. Remote Sens.*, vol. 169, pp. 214–226, 2020, doi: https://doi.org/10.1016/j.isprsjprs.2020.09.009.

[17] D. Pandey and K. C. Tiwari, "Extraction of urban built-up surfaces and its subclasses using existing built-up indices with separability analysis of spectrally mixed classes in AVIRIS-NG imagery," *Adv. Sp. Res.*, vol. 66, no. 8, pp. 1829–1845, 2020, doi: https://doi.org/10.1016/j.asr.2020.06.038.

[18] W. Xia, Z. Chen, Y. Zhang, and J. Liu, "An Approach for Road Material Identification by Dual-Stage Convolutional Networks 1 China Transport Telecommunications & Information Center , Beijing 100011 , China , 2 School of Computer Science and Technology , Donghua University , Shanghai 201620 , China," pp. 7153–7156, 2018.

[19] H. Baluyan, B. Joshi, A. Al Hinai, and W. L. Woon, "Novel Approach for Rooftop Detection Using Support Vector Machine," *ISRN Mach. Vis.*, vol. 2013, pp. 1–11, 2013, doi: 10.1155/2013/819768.

[20] M. Jilge, U. Heiden, C. Neumann, and H. Feilhauer, "Gradients in urban material composition: A new concept to map cities with spaceborne imaging spectroscopy data," *Remote Sens. Environ.*, vol. 223, pp. 179–193, 2019, doi: https://doi.org/10.1016/j.rse.2019.01.007.

[21] O. Okwuashi and C. E. Ndehedehe, "Deep support vector machine for hyperspectral image classification," *Pattern Recognit.*, vol. 103, p. 107298, 2020, doi: https://doi.org/10.1016/j.patcog.2020.107298.

[22] L. M. Francis and N. Sreenath, "TEDLESS – Text detection using least-square SVM from natural scene," *J. King Saud Univ. - Comput. Inf. Sci.*, vol. 32, no. 3, pp. 287–299, 2020, doi: https://doi.org/10.1016/j.jksuci.2017.09.001.

[23] R. Bhuvaneswari and R. Subban, "Novel object detection and recognition system based on points of interest selection and SVM classification," *Cogn. Syst. Res.*, vol. 52, pp. 985–994, 2018, doi: https://doi.org/10.1016/j.cogsys.2018.09.022.

[24] A. Chitlangia and G. Malathi, "Handwriting Analysis based on Histogram of Oriented Gradient for Predicting Personality traits using SVM," *Procedia Comput. Sci.*, vol. 165, pp. 384–390, 2019, doi: https://doi.org/10.1016/j.procs.2020.01.034.

[25] L. Blanchet *et al.*, "Constructing bi-plots for random forest: Tutorial," *Anal. Chim. Acta*, vol. 1131, pp. 146–155, 2020, doi: https://doi.org/10.1016/j.aca.2020.06.043.

[26] S. Wangchuk and T. Bolch, "Mapping of glacial lakes using Sentinel-1 and Sentinel-2 data and a random forest classifier: Strengths and challenges," *Sci. Remote Sens.*, vol. 2, p. 100008, 2020, doi: https://doi.org/10.1016/j.srs.2020.100008.

[27] M. Wainberg, B. Alipanahi, and B. J. Frey, "Are random forests truly the best classifiers?," vol. 17, pp. 1–5, 2016.

[28] S. Ghosh and A. Das, "Wetland conversion risk assessment of East Kolkata Wetland: A Ramsar site using random forest and support vector machine model," *J. Clean. Prod.*, vol. 275, p. 123475, 2020, doi: https://doi.org/10.1016/j.jclepro.2020.123475.

[29] Z. Fu and A. Robles-Kelly, "Discriminant Absorption-Feature Learning for Material Classification," *Geosci. Remote Sensing, IEEE Trans.*, vol. 49, pp. 1536–1556, 2011, doi: 10.1109/TGRS.2010.2086462.

[30] R. M. Parish, "The Application of Visible / Near-Infrared Reflectance (VNIR) Spectroscopy to Chert : A Case Study from the Dover Quarry Sites , Tennessee," vol. 26, no. 3, pp. 420–439, 2011, doi: 10.1002/gea.20354.

[31] S. Li, H. Wu, D. Wan, and J. Zhu, "Knowledge-Based Systems An effective feature selection method for hyperspectral image classification based on genetic algorithm and support vector machine," *Knowledge-Based Syst.*, vol. 24, no. 1, pp. 40–48, 2011, doi: 10.1016/j.knosys.2010.07.003.

[32] W. Heldens, T. Esch, U. Heiden, and S. Dech, "Potential of hyperspectral remote sensing for characterisation of urban structure in Munich," 2008, pp. 94–103.

[33] Astrium, *Pléiades Imagery User Guide*, no. October. 2012.

[34] X. Meng, H. Shen, H. Li, L. Zhang, and R. Fu, "Review of the pansharpening methods for remote sensing images based on the idea of meta-analysis: Practical discussion and challenges," *Inf. Fusion*, vol. 46, pp. 102–113, 2019, doi: https://doi.org/10.1016/j.inffus.2018.05.006.
[35] M. Ehlers, "Multisensor image fusion techniques in remote sensing," *ISPRS J. Photogramm. Remote Sens.*, vol. 46, no. 1, pp. 19–30, 1991, doi: https://doi.org/10.1016/0924-2716(91)90003-E.
[36] A. E. Bayá and M. G. Larese, "Pixel sampling by clustering," *Expert Syst. Appl.*, vol. 159, p. 113576, 2020, doi: https://doi.org/10.1016/j.eswa.2020.113576.
[37] Astrium, "SPOT 6 & SPOT 7 Imagery User Guide," no. July, 2013.
[38] C. Lei *et al.*, "A comparison of random forest and support vector machine approaches to predict coal spontaneous combustion in gob," *Fuel*, vol. 239, pp. 297–311, 2019, doi: https://doi.org/10.1016/j.fuel.2018.11.006.